J Forensic Sci, March 2007, Vol. 52, No. 2
doi:10.1111/j.1556-4029.2006.00354.x
Available online at: www.blackwell-synergy.com

Jennifer R. Verkouteren,[1] *M.S.*

Particle Characteristics of Trace High Explosives: RDX and PETN*

ABSTRACT: The sizes of explosives particles in fingerprint residues produced from C-4 and Semtex-1A were investigated with respect to a fragmentation model. Particles produced by crushing crystals of RDX and PETN were sized by using scanning electron microscopy, combined with image analysis, and polarized light microscopy was used for imaging and identifying explosive particles in fingerprint residues. Crystals of RDX and PETN fragment in a manner that concentrates mass in the largest particles of the population, which is common for a fragmentation process. Based on the fingerprints studied, the particle size to target for improving mass detection in fingerprint residues by ion mobility spectrometry (IMS) is $\geq 10\,\mu m$ in diameter. Although particles smaller than $10\,\mu m$ in diameter have a higher frequency, they constitute $<20\%$ of the total mass. Efforts to improve collection efficiency of explosives particles for detection by IMS, or other techniques, must take into consideration that the mass may be concentrated in a relatively few particles that may not be homogeneously distributed over the fingerprint area. These results are based on plastic-bonded explosives such as C-4 that contain relatively large crystals of explosive, where fragmentation is the main process leading to the presence of particles in the fingerprint residues.

KEYWORDS: forensic science, RDX, PETN, explosives, particle sizes, fingerprints, IMS

The search for traces of explosives on people and objects at airports and other points of entry as a preventative, antiterrorist measure has accelerated in recent years, and one of the commonly used techniques is ion mobility spectrometry (IMS). The detection of the high explosives RDX (cyclotrimethylene trinitramine) and PETN (pentaerythritol tetrantitrate) by IMS is dependent on the collection of solid particles because of the relatively low vapor pressures of the two high explosives. Handling of plastic-bonded explosives such as composition C-4 (RDX plus binders) and Semtex-H (PETN and RDX plus binders) is expected to produce fingerprint residues containing particles of explosives on objects such as clothing, hair, luggage, laptop computers, etc. Particle collection is accomplished for the tabletop IMS instruments by wiping surfaces with fabric or paper traps that are placed directly in the instrument. For walk-through portal IMS systems (1), directed air jets and/or natural convection processes are used to dislodge and transport the particles. Of critical importance to the design of both types of collection schemes is the size of particles expected in the residues. This is particularly true for portal systems, where particle size affects not only removal efficiencies but also transport to and collection by the filters on the front end of the detector system. Because IMS is mass dependent, detection efficiency is improved by targeting those particle sizes that carry the majority of the mass of the population, and not simply those particle sizes that have the highest frequency. Therefore, it is important to understand both the particle size distribution of explosives in fingerprint residues, and the distribution of mass with respect to particle size.

The particle sizes of feedstock powders of RDX and PETN used in the manufacture of plastic-bonded explosives can range from nanometers to millimeters depending on the type of crystallization process used. Military specifications for C-4 require feedstock RDX with a 3:1 mix of two particle sizes with diameters of 850 and 44 μm, respectively (2). When handling C-4 and Semtex, the main process leading to the presence of particles in residues is probably fragmentation of the crystals, resulting in much smaller particles in the residues than in the parent material. Fragmentation is a physical process known to give rise to a power-law particle size distribution (3,4), suggesting the possibility of modeling particle sizes in residues.

An earlier study of particle sizes in C-4 fingerprint residues reported a bimodal distribution with one mode at *c.*100 μm, and a second at 250 μm (5). This earlier study did not discriminate RDX from the fuel oil and elastomers also present in C-4, or from oils and other components naturally present in fingerprint residues. Because detection is based on the presence of the explosive, our study was designed to investigate the particle sizes of the explosive, as separate from the other components, in both C-4 and Semtex-1A fingerprints, although the argument can be made that the explosive particles may not be physically separable for collection purposes.

Fragmentation

Fragmentation processes, including grinding, crushing, impact, and explosion, are known to produce particle size distributions that follow a power law, as reported for many different materials including asteroids (6), soils (4), and asbestos (7). Power-law size distributions have been interpreted to indicate a fractal, i.e. scale invariant, process given by

$$N = Cd^{-D}$$

where C is a constant, N is the number of objects with a diameter greater than d, and D is the fractal dimension. A log transformation results in

$$\log N = -D(\log d) + C$$

[1]Chemical Science and Technology Laboratory, National Institute of Standards and Technology, Gaithersburg, MD.

*This work was presented orally at 8th ISADE, International Symposium on the Analysis and Detection of Explosives, Ottawa, Canada, June 6–10, 2004.

Received 25 Mar. 2006; and in revised form 9 July 2006; accepted 14 July 2006; published 30 Jan. 2007.

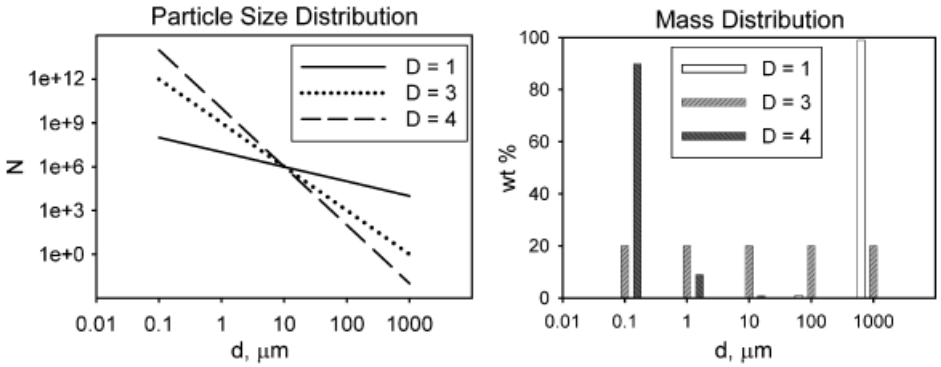

FIG. 1—*Schematic examples of three different fractal dimensions plotted as the cumulative frequency (N) versus diameter, and the resulting mass distributions.*

such that the fractal dimension is the slope of the line of the cumulative size distribution with respect to size, as shown in Fig. 1. The theoretical range for D is between 0 and 3 (3), and most measurements of earth materials fall within this range with some exceptions (4). The fractal dimension is sensitive to material type and is a measure of the resistance to fragmentation; it is relatively insensitive to the method or duration of fragmentation (4). Varying the input energy or duration of fragmentation does not alter the fractal dimension, but changes the limits of the size distribution. Although a single fractal dimension works for many materials, soils are more complicated and are often described by multiple fractal dimensions (8–10). More recent work on some asteroid populations has also indicated the possibility of multifractal behavior (11).

To determine the total mass of a particle population, and therefore the distribution of mass with particle size, the limits of the distribution, d_{min} and d_{max}, must be known. For demonstration purposes, the mass distributions were computed for three particle distributions with $d_{min} = 0.1$ μm and $d_{max} = 1000$ μm, assuming a common three-dimensional shape for all size fractions and a constant density, as shown in Fig. 1. For the range of normal fractal dimensions, mass is generally concentrated in the large particle end, as shown for the computed mass distribution for $D = 1$. It has been theoretically demonstrated that for three-dimensional particles with $D \leq 3$, only the large particle limit of the distribution must be known in order to obtain a reasonable approximation of the total mass; for distributions with $D>3$, only d_{min} must be known (12).

Experimental Procedure

The fragmentation properties of RDX and PETN were determined by extracting explosive crystals from samples of plastic explosive, crushing them, and then sizing the particles using scanning electron microscopy (SEM). From these data, the fractal dimensions could be evaluated to determine the distribution of mass with particle size. Additional experiments were conducted by handling the plastic explosives and forming fingerprints from residues left on the hands. Polarized light microscopy (PLM) was used to size the explosives particles in the fingerprints. Although SEM has superior spatial resolution, it was not used for analyzing particles in fingerprints because the explosive compounds could not be discriminated from overlying binder materials. PLM was capable of discriminating RDX and PETN from binder in C-4 and Semtex-1A, and was used for the analysis of the fingerprints.

Particle Sizing by SEM

Samples of C-4 and Semtex-1A were obtained from the Transportation Security Administration. Semtex-1A contains only PETN as the high explosive (13), and not the mix of PETN and RDX that is present in the more common Semtex-H. SEM images of representative portions of the samples are shown in Fig. 2 and illustrate crystal shapes and sizes. The crystals of RDX in C-4 and of PETN in Semtex-1A range in size from a few micrometers to a few millimeters. Some of the larger crystals were extracted with tweezers from each sample and scraped clean of binders. Three crystals each of RDX and PETN were crushed separately in glass beakers with a glass stirring rod. Prefiltered hydraulic fluid was added to each beaker to disperse the particles, and the solutions were placed in an ultrasonic bath for 10 min. The particles were collected by filtration onto 0.1 μm polycarbonate filters and rinsed with heptane to remove residual hydraulic fluid. The particle filters were coated by plasma deposition with a AuPd alloy to prevent charging during SEM analysis.

The filters were analyzed with a Hitachi field emission gun SEM (Hitachi High Technologies America, Pleasanton, CA) at three magnifications for RDX and four magnifications for PETN to cover the size range down to 1 μm. (Certain commercial equipment, instruments, or materials are identified in this document that does not imply recommendation or endorsement by the National Institute of Standards and Technology, nor does it imply that the products identified are necessarily the best available for the purpose.) Backscattered electron images of 50 randomly selected fields were collected at each magnification. Each magnification was calibrated with an MRS-3 Geller NIST-traceable SEM (Geller Microanalytical Laboratory, Topsfield, MA) size standard. A representative image of PETN at $\times$ 500 magnification is shown in Fig. 3; both PETN and RDX particles are bright under these imaging conditions and can be segregated using a simple thresholding process. Images were processed with the software package Image-Pro, and the size of each particle was calculated from the thresholded area as the average length of diameters measured at 2° intervals and passing through the object's centroid. Particles touching the boundary of the image were not counted. Particles were binned by diameter into 1 μm bins, and the frequency in each bin was converted to a total count using the ratio of filter area sampled at that magnification to the active filter area.

The magnifications were chosen to provide overlap of many of the size bins in order to evaluate counting errors. For the lower magnifications, the primary source of counting error is resolution, whereas for the higher magnifications, the primary source of error is in the limited sampling of the filter. Higher magnifications provide better size resolution, but sample a smaller area, and

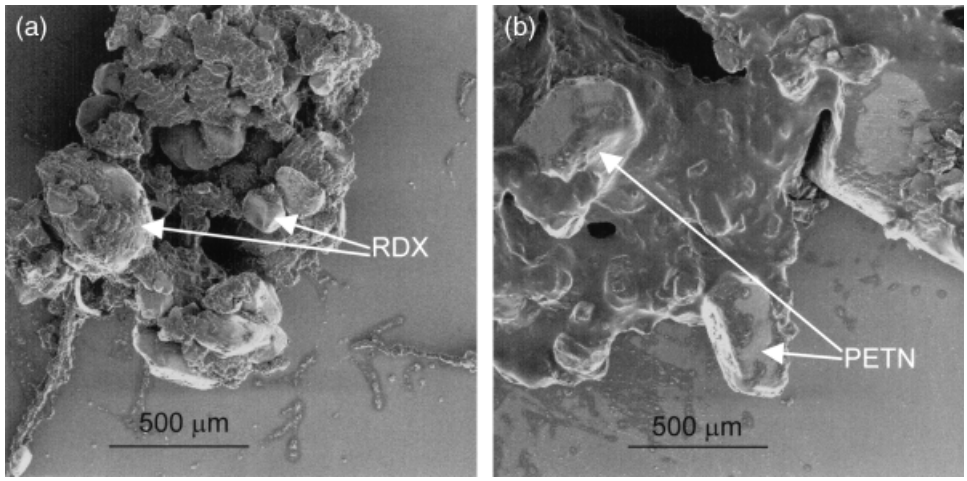

FIG. 2—*SEM images of samples used in this study; (a) C-4 and (b) Semtex-1A. Both samples contain crystals of explosive in a binder of oils and elastomers.*

therefore the extrapolation from the number of counted particles to the number for the entire filter is larger. For those bins represented by data from more than one magnification, the frequency was calculated as the mean, and the errors calculated as the standard deviation.

Particle Sizing in Fingerprints

To generate fingerprints, small portions of the C-4 and Semtex-1A samples were handled and then all visible material was removed from the hands. A series of 10 fingerprints of each explosive type was produced by successively impressing one finger on precleaned glass slides for analysis by PLM. Only the first and tenth fingerprints, referred to subsequently as first and tenth generation, of each explosive type were analyzed.

The optical properties of RDX and PETN as reported by McCrone et al. (14) were used to differentiate particles of explosive compounds from matrix materials. A drop of immersion oil was placed on the fingerprint residue and covered by an 18 mm square cover slip to provide a constant area to count. RDX was distinguished from other C-4 components due to its high optical birefringence, which results in bright RDX crystals under crossed polarized light (Fig. 4). The other components of C-4, and those naturally present on skin, generally have lower birefringences or are isotropic (dark under crossed polarized light) and therefore are readily distinguished from RDX. The one interference noted was organic fibers that are present in C-4 and other plastic explosives; these could be distinguished on the basis of their shape.

PETN has a relatively low birefringence, and could not be differentiated from the other components in fingerprint residues on that basis. Instead, an index-matching technique was used for PETN by matching the refractive index of the immersion oil to that of PETN, using a liquid with a refractive index $n_D = 1.552$. The refractive index of PETN particles could be confirmed by comparison with the liquid, allowing a positive identification to be made. This method of differentiating PETN resulted in a limited resolution by PLM compared with the method used for RDX, because an index-matching technique necessarily reduces the visibility of the material.

The area under the cover slip was scanned in its entirety at $\times$ 200 magnification to determine a total particle count. The minimum particle size for counting purposes was 2 μm for RDX

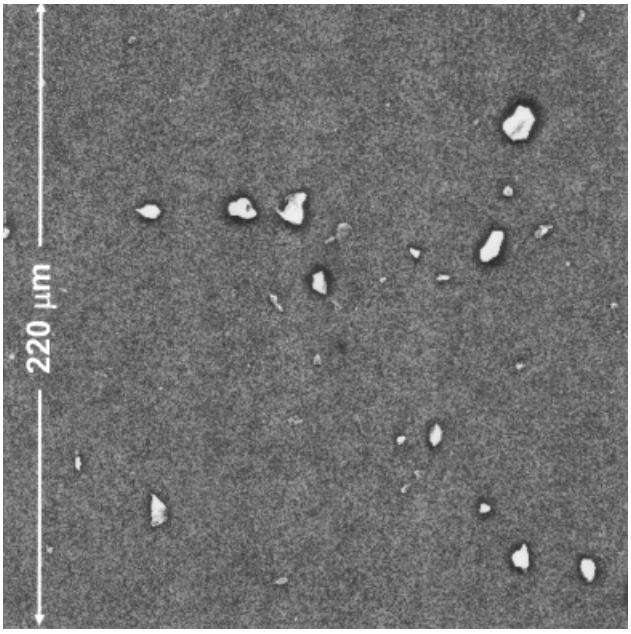

FIG. 3—*Backscattered electron image at $\times$ 500 magnification of PETN particles produced by crushing crystals extracted from Semtex-1A.*

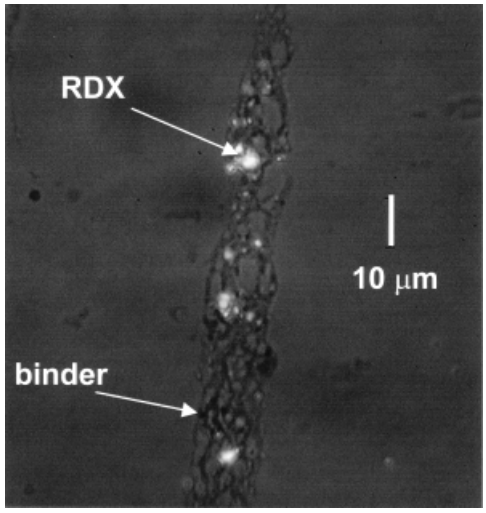

FIG. 4—*Polarized light microscope image of birefringent (bright) RDX particles encased in binder material in the first-generation fingerprint of C-4.*

and 5 μm for PETN. Particle sizes were determined by comparison with a 50 μm reticle scale bar calibrated against a stage micrometer, estimating the diameter of the particle assuming a round particle. This visual estimation method of particle counting was used in preference to image analysis because it allowed for a relatively rapid and complete scanning of the entire deposit. The particle distribution was very inhomogeneous within the fingerprint, and a selected number of images would not have been representative. The number of images required for complete coverage was impractical, given the instrumental setup. The errors in particle sizing using visual estimation were evaluated by comparison with image analysis results for 10 fields, and are ± 10% for particles larger than 10 μm, and ± 50% for particles smaller than 10 μm. Uncertainties were estimated for the PLM particle counts by creating two additional sets of data: one where 10% is added to the size of each particle larger than 10 μm, and 50% is added to the size of each particle smaller than 10 μm, and a second set where those values are subtracted from each particle size. Each data set was binned, and the standard deviation for the three values in each bin was used as the estimate of uncertainty. These uncertainties are assumed to be conservative, as one would not expect the bias to operate in the same direction for each size bin, thereby enlarging the error.

Results

The SEM particle sizing data from the crushed crystals of PETN and RDX are shown in Fig. 5. The range of sizes between 1 and 20 μm had a significant overlap among the magnifications used, from which the uncertainties were derived as discussed previously. The larger particles could only reasonably be counted at the lowest magnification (× 150), and the 50 fields collected at × 150 covered *c*.10% of the active filter area. Because the larger particles were sampled at only one magnification, their frequencies were corrected for bias due to exclusion of particles touching the boundaries of the image. This correction uses a ratio of the particle size to the image size and accounts for the effective reduction in sampled area (15). Particles were well dispersed, as can be seen in Fig. 3, and therefore particle sizing is not significantly affected by particle agglomeration during filter preparation. Images of both RDX and PETN were taken at higher magnifications to evaluate the frequency of particles < 1 μm in diameter. Many more than 50 images would have been required to achieve reasonable counting statistics at these magnifications, and so only a qualitative assessment was performed. Based on the assessment, the frequencies of the particles < 1 μm in diameter appear to be consistent with the numbers obtained by extrapolation of the data.

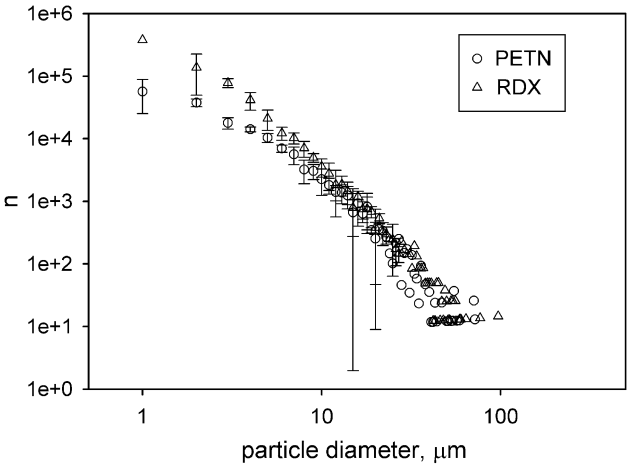

FIG. 5—*Frequency (n) of particle sizes binned in 1* μm *bins from scanning electron microscopy data. Uncertainties given for size bins with overlapping data from two or more magnifications, calculated as the standard deviation of the mean.*

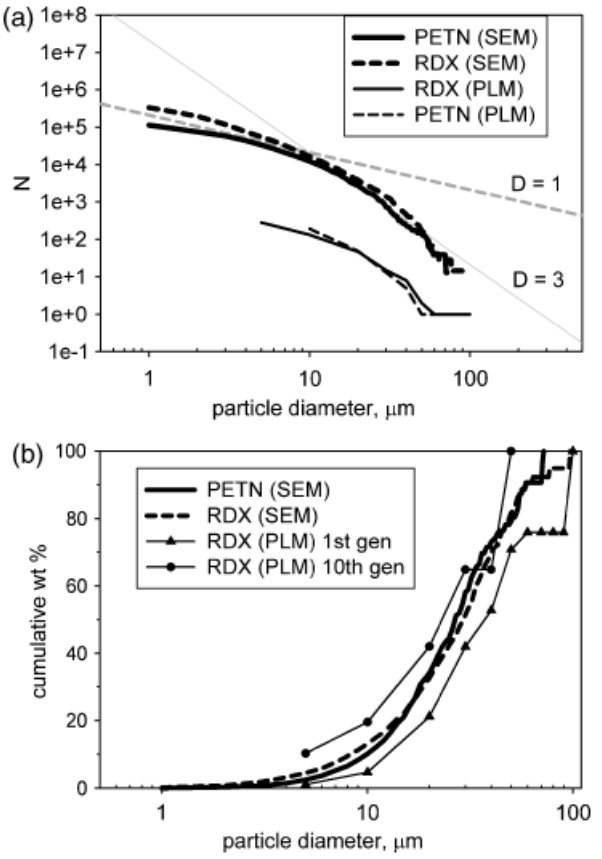

FIG. 6—*(a) Cumulative frequency (N) of particle sizes calculated from scanning electron microscopy (SEM) data and from PLM fingerprint data (first generation). Dashed lines represent fractal dimensions D = 1 and 3. (b) Mass distributions computed as cumulative wt% from particle size distributions, assuming a common shape for all sizes.*

The cumulative size distributions for PETN and RDX, computed from the SEM data presented in Fig. 5, are given in Fig. 6*a*, where each bin has the cumulative frequency (*N*) of all the particles larger than that bin size. It is clear that a single fractal dimension cannot be determined for either PETN or RDX, as neither distribution is linear. The data can best be described as multifractal, with $D \approx 3$ for particles larger than *c*. 10 μm, and $D \approx 1$ for particles smaller than *c*. 10 μm. This multifractal behavior may be due to a change from brittle to non-brittle fragmentation. Materials generally exhibit a grinding limit at some particle size below which it is difficult to further reduce the size because of a change from brittle to plastic deformation (16). The fingerprint data also contain some evidence of plastic deformation, particularly in the case of PETN, as described later.

In any case, it is clear from the fractal analysis that the mass will not be concentrated in the smallest particles in the distribution, particularly those < 10 μm in diameter. This is demonstrated graphically in Fig. 6*b*, where the cumulative wt% of each size bin is calculated assuming a common particle shape for all sizes. (It does not matter what particle shape is assumed, as long as the shape does not vary with size.) If the SEM data are extrapolated to include 0.1 μm as the lower limit with a frequency twice that of the 1 μm size bin, the mass distributions shown in Fig. 6*b* remain

essentially unchanged. For these populations of PETN and RDX, the particles smaller than 10 μm constitute <20% of the total mass.

From these results, we conclude that the largest particles that are present in fingerprint residues of C-4 and Semtex-1A will guide the selection of particle sizes to target for IMS collection. Our data for first-generation prints of the samples of C-4 and Semtex-1A studied here show that the largest particles of RDX and PETN are between 50 and 100 μm in size, as shown in Fig. 7. The particles are primarily single particles and not complex agglomerations. In general, the size of the largest particles will be dependent on the size of the starting material to be fragmented and on the force of the fragmentation. One would expect the tenth-generation fingerprint to have a smaller maximum particle size than the first-generation print, which is the case for the C-4 fingerprints. The maximum particle size of PETN appears to increase with fingerprint generation, but this is a result of a change in particle shape. The PETN particles smear into thin, flat plates as the fingerprint generation increases, consistent with the non-brittle deformation suggested by the multifractal behavior. The smallest bin size may be undercounted in the fingerprint data because of PLM resolution limitations, particularly in the case of PETN. However, the cumulative frequency distributions are quite similar to those derived from the SEM data (Fig. 6*a*), although the absolute frequencies are much lower. This similarity of the distributions suggests that fragmentation is a reasonable explanation for the presence of explosives in fingerprint residues. The distribution of mass with respect to particle size for the C-4 prints is shown in Fig. 6*b*; the particles 10 μm or less in size represent <10% of the total mass in the first-generation print, and *c*. 20% of the mass in the tenth-generation print. The mass was not determined for PETN because of the problem with flattened particles, which implies that a constant shape approximation is not reasonable.

The total mass of RDX in the C-4 fingerprints calculated from the particle distribution is dependent on the assumed shape of the particles. An expected range of masses given two endpoint shapes, either that the height is 10% of the width, or that the particles are spherical, is 0.3–4 μg for the first generation, and 26–340 ng for the tenth generation, assuming a density of 1.8 g/cm^3 (17). A reasonable assumption is that the height is 50% of the width; in that case, the first-generation print has 1.5 μg of RDX, and the tenth-generation print has 130 ng. These values are generally consistent with the average values of RDX in first- and tenth-generation fingerprints of C-4 reported by Gresham et al. (5) of 3 μg and 129 ng, respectively. This general concurrence indicates that the fingerprints described here are not inconsistent with a larger population of C-4 fingerprints. This point bears further study, and work is continuing in this area to describe a wider population of samples.

Targeting particles 10 μm and larger for collection would be appropriate for the fingerprints studied here. A factor that must be considered when mass is concentrated in a relatively few large particles is the area distribution of those particles. In the fingerprints measured in this study, inhomogeneities were observed wherein large particles of RDX and PETN tended to be concentrated in small areas. For example, the image shown in Fig. 8 for RDX in the first-generation C-4 fingerprint represents only 0.4% of the total fingerprint area, but contains 32% of all particles that are 20 μm in diameter or larger, or 26% of the total mass. This implies a fairly stringent requirement for effective sampling during swipe sampling to cover the entire area represented by the fingerprint. This problem becomes more apparent as the total particle count decreases. For example, there are only 14 RDX particles 20 μm or larger in the tenth-generation C-4 print, and the single 50 μm particle accounts for 35% of the mass.

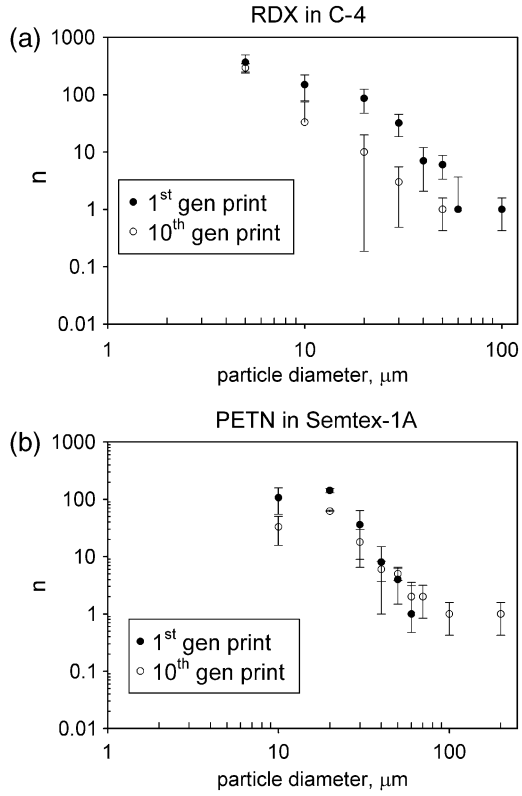

FIG. 7—*Frequency (n) of explosives particles counted by polarized light microscopy in first- and tenth-generation fingerprints of (a) C-4 and (b) Semtex-1A. Uncertainties calculated as the standard deviation of the mean.*

Discussion

With the large crystals of RDX and PETN present in the C-4 and Semtex-1A samples used in this study, it is reasonable to assume that fragmentation is the primary process for generating particles in the fingerprint residues. Under these conditions, the mass of the particle population in first- to tenth-generation fingerprint residues is heavily concentrated in particles 10 μm in diameter or larger, and the maximum particle sizes are 50–100 μm.

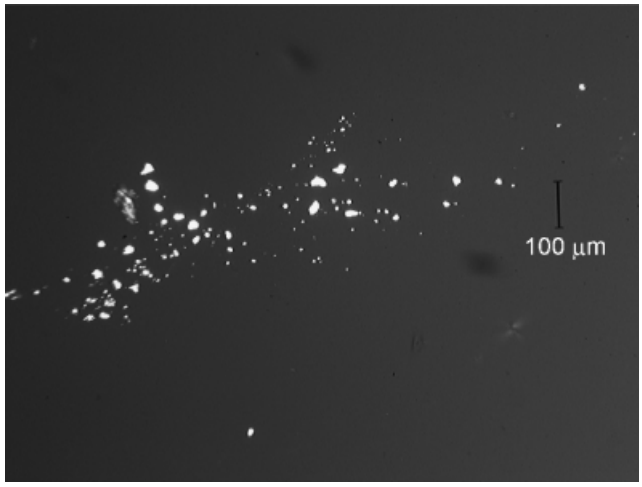

FIG. 8—*Concentration of large RDX particles in a first-generation C-4 print.*

The feedstock particles in these explosive formulations have dimensions exceeding 100 μm. However, there is a range of particle sizes in explosive feedstock powders, including an ultrafine (≤ 5 μm) category of RDX. Particle size is one of the factors that affects the performance characteristics of explosives, and various recrystallization processes may be used to control the mean particle size and the particle size distribution (18,19), and even to produce nano-sized materials (20). In addition, there are processing procedures during manufacture that serve to reduce the size of the original feedstock powders in materials such as Detasheet® (Dupont, Wilmington, DE), one of the plastic-bonded explosives formed as sheet goods.

If the particles are small enough in the plastic-bonded explosive, they may be transferred intact to the residue and therefore have the size distribution inherent to the feedstock powder. Size distributions from crystallization processes are much different from those produced by fragmentation, and the mass of the population is likely to be concentrated at the mean particle size, rather than with the largest particles. Although the results reported here point to a target particle size of 10 μm or larger, if processing conditions have reduced the largest particle size in the plastic-bonded explosive, the largest particle size in the residue will also necessarily be reduced. Future work involves study of a large sample set of plastic-bonded explosives to determine the variability in maximum particle sizes in residues as a result of variability in the starting materials. Work is already underway to measure particle heights in order to evaluate shape characteristics. In addition, other mechanisms of transfer other than by fingerprints will be considered.

References

1. Hallowell SF. Screening people for illicit substances: a survey of current portal technology. Talanta 2001;54:447–58.
2. Davies JP, Hallowell SF, Hoglund DE. Particle generators for the calibration and testing of narcotic and explosive vapor/particle detection systems. In: Harding GL, Lanza RC, Myers LJ, Young PA, editors. Proceedings of SPIE: substance detection systems, Vol. 2092. Innsbruck, Austria: The International Society for Optical Engineering, 1994:137–44, http://spiedl.aip.org/browse/vol_range.jsp.
3. Turcotte DL. Fractals and fragmentation. J Geophys Res 1986;91(B2):1921–6.
4. Perfect E. Fractal models for the fragmentation of rocks and soils: a review. Eng Geol 1997;48:185–98.
5. Gresham GL, Davies JP, Goodrich LD, Blackwood LG, Liu BYH, Thimsem D et al. Development of particle standards for testing detection systems: mass of RDX and particle size distribution of composition 4 residues. In: Lawrence AH, editor. Proceedings of SPIE: cargo inspection technologies, Vol. 2276. San Diego, CA: The International Society for Optical Engineering, 1994:34–44, http://spiedl.aip.org/browse/vol_range.jsp.
6. Dohnanyi JS. Collisional model of asteroids and their debris. J Geophys Res 1969;74:2531–54.
7. Wylie AG. Modeling asbestos populations: a fractal approach. Can Mineral 1993;30:437–46.
8. Posada AND, Gimenez D, Bittelli M, Vaz CMP, Flury M. Multifractal characterization of soil particle-size distributions. Soil Sci Soc Am J 2001;65:1361–7.
9. Bittelli M, Campbell GS, Flury M. Characterization of particle-size distribution in soils with a fragmentation model. Soil Sci Soc Am J 1999;64:782–8.
10. Grout H, Tarquis AM, Wiesner MR. Multifractal analysis of particle size distributions in soil. Environ Sci Technol 1998;32:1176–82.
11. Bagatin AC, Martinez VJ, Paredes S. Multifractal fits to the observed main belt asteroid distribution. Icarus 2002;157(2):549–53.
12. Carpinteri A. One, two, and three-dimensional universal laws for fragmentation due to impact and explosion. Trans ASME 2002;69:854–6.
13. Tarver CM, Tran TD, Whipple RE. Thermal decomposition of pentaerythritol tetranitrate. Propell Explos Pyrot 2003;28(4):189–93.
14. McCrone WC, Andreen JH, Tsang S. Identification of organic high explosives. Microscope 1993;41:161–82.
15. Terry KW. Particle size distribution of airborne dusts using a scanning electron microscope. Aerosol Sci Technol 1995;23:475–8.
16. An LJ, Sammis CG. Particle size distribution of cataclastic fault materials from southern California: a 3-D study. Pure Appl Geophys 1994;143(1–3):203–27.
17. Hoffman DM. Density distributions of cyclotrimethylenetrinitramines (RDX). Destin (FL): Joint Army Navy NASA Air Force 38th Combustions Subcommittee, 26th Airbreathing Propulsion Subcommittee, 20th Propulsion Systems Hazards Subcommittee, and 2nd Modeling and Simulation Subcommittee; 2002 March, U.S. Department of Energy Report: UCRL-JC-147684:1–16.
18. Teipel U. Production of particles of explosives. Propell Explos Pyrot 1999;24:134–9.
19. Gallagher PM, Coffey MP, Krukonis VJ, Hillstrom WW. Gas anti-solvent recrystallization of RDX: formation of ultra-fine particles of a difficult-to-comminute explosive. J Supercrit Fluid 1992;5:130–42.
20. Gomez LM, Hernandez SP, Mina N, Lareau RT, Chamberlain RT, Castro ME. Synthesis and characterization of monodispersed 300 nm RDX particles. In: Proceedings of the 226th National Meeting of the American Chemical Society, New York, NY, Vol. 226. Washington, DC: American Chemical Society, 2003:U327–84, Phys Part 2, 2003.

Additional information and reprint requests:
Jennifer R. Verkouteren, M.S.
National Institute of Standards and Technology (NIST)
100 Bureau Dr. Mailstop 8371
Gaithersburg, MD 20899-8371
E-mail: jennifer.verkouteren@nist.gov